Influence of the Atmospheric Channel on the Sound Propagation above the Ground Surface

Prof. Nikolai P. Krasnenko
Tomsk State University of Control Systems and Radioelectronics,
40, Lenin av., Tomsk, 634050, Russia
Institute of Monitoring of Climatic and Ecological Systems SB Russian Academy of Sciencies,
10/3, Akademicheskii av., Tomsk, 634055, Russia

E-mail: krasnenko@iom.tomsknet.ru

SUMMARY

In this paper are presented the results of investigations into the influence of the atmospheric channel on the sound propagation above the ground surface.

The algorithms for calculating the sound pressure level and the software package Outdoor Acoustics intended for real-time estimate of the field of the mean sound pressure level from a remote sound sourse in the ground atmospheric layer have been described. The software package allows for the characteristics of the sound source, vertical profiles of the main meteorological parameters, characteristics of the underlying surface, and the parameters of the atmospheric turbulence.

Results of numerical estimation and field tests of this software package for distancies from an acoustic source up to 6 km are also presented in the paper.

1 INTRODUCTION

It is well known that the atmospheric sound pressure level recorded from a stationary source essentially depends on meteorological conditions. This is caused by the high sensitivity of total energetic sound losses to such meteorological parameters as wind, temperature, relative air humidity, and atmospheric pressure. Mean values of air humidity, temperature, and pressure determine not only the coefficient of molecular absorption of the acoustic radiation at a fixed frequency, but also its frequency dependence (Brown and Hall, 1978; Harris, 1966). Fluctuations of the acoustic refractive index, caused by turbulent pulsations of the meteorological parameters, affect an interference pattern of directly transmitted and reflected acoustic rays and cause the excess turbulent attenuation (Brown and Hall, 1978; Ingard, 1953). In case of near-ground sound propagation at distances more than 1 km, sound attenuation is primarily affected by refraction on gradients of temperature and wind (Ostashev, 1992), resulting in the waveguide or nonwaveguide regime of sound propagation. In the first case, rays bend downward and hence undergo multiple reflections from the ground (Figure 1b). Relatively small values of sound attenuation are typical of this regime of sound propagation. In the second case, rays bend upward, and a shadow zone is formed near the ground at certain distances from the source (Figure 1c). Only very weak sound, caused by turbulent scattering in the upper atmospheric layers, penetrates into this zone.

In the present paper, we describe algorithms for calculating the mean sound pressure level in the surface layer of the atmosphere considering the effect of meteorological conditions on sound propagation. The software package Outdoor Acoustics, developed on the basis of these algorithms, is also outlined in the paper together with the results of its application to field measurements and quantitative estimations of the effect of the most important meteorological factors on sound attenuation.

Paper presented at the RTO SET Symposium on "Capabilities of Acoustics in Air-Ground and Maritime Reconnaissance, Target Classification and Identification", held in Lerici, Italy, 26-28 April 2004, and published in RTO-MP-SET-079.

Some results were presented in our previous papers (Bogushevich and Krasnenko, 1993; Abramov et al., 1994; Bogushevich and Krasnenko, 1996; 1997; 1998).

2 ALGORITHM FOR CALCULATING THE SOUND PRESSURE LEVEL FOR LINE-OF-SIGHT PROPAGATION

A regime of weak refraction (called neutral below) is the most simple case of line-of-sight propagation of an acoustic wave to an observation point. In this regime, only two rays come to the observation point: a direct ray and a ray reflected from the ground; in this case, the direct ray does not have any bending point (see Figure 1a). In the neutral regime a ray pattern of sound propagation is characterized by insignificant bending of ray trajectories. It can be observed only for small gradients of wind velocity and temperature or short distances d to the observation point. For the neutral regime, the sound pressure level can be calculated neglecting the effect of refraction by the algorithm

$$L_r(f) = L_s(f) + L_{abs}(f) + L_t(f) + L_e(f) + L_{div}(f) + L_{pat}(f), \tag{1}$$

where $L_r(f)$ is the sound pressure level at the observation point r at the frequency f, in dB; L_s is the sound pressure produced by a source and adjusted to a distance of 1 m from the source; L_{abs} allows for the contribution of classical and molecular sound absorption in air; L_t specifies the contribution of turbulent sound attenuation; L_e allows for the contribution of the Earth's surface (it allows for the interference between the directly transmitted and reflected waves); L_{div} specifies the contribution of angular divergence of sound wave (for the examined regime, it is spherical divergence); $L_{pat} = 10 \log[F(\alpha, \varphi, f)]$ is the term that allows for the normalized directional pattern of the source $F(\alpha, \varphi, f)$.

All terms in the right side of Eq. (1) except L_s, as a rule, are negative. Relation (1) expresses the wave energy conservation law and is the equation of energy balance. Algorithms for calculation of individual components of sound attenuation are described in the literature in detail (see, for example, Krasnenko, 1986). We note that when sound propagates at distances longer than 1 km, the neutral regime is practically not observed.

When analyzing the waveguide sound propagation, the rays which enter the given point for existing wind velocity profiles $\mathbf{v}(z)$ and sound velocity in the air $c(z)$ are calculated. This analysis is carried out on the basis of the equation describing the horizontal coordinates $\mathbf{r} = \mathbf{r}(x, y)$ of each point of a ray which is characterized by the angles of ray departure α and φ in two orthogonal planes. Assuming that the mean vertical component of wind velocity v_z equals zero, the ray path equation has the form (Ostashev, 1989):

$$\mathbf{r} = \mathbf{r}_0 + \int_{z_<}^{z_>} \frac{\mathbf{K} \cdot \dfrac{\mathbf{V}}{c} + \mathbf{a}}{q} \, \mathrm{d}z, \tag{2}$$

where $\mathbf{r}_0$ are the horizontal coordinates of the ray emission point; $z_<$ and $z_>$ are the altitudes of the lower and upper points of the ray trajectory; $K(z) = [\omega - \mathbf{a} \cdot \mathbf{v}(z)]/c(z)$ is the wave number in a moving medium; $q(z) = \sqrt{K^2(z) - \mathbf{a}^2}$ is the vertical component of wave vector $\mathbf{K}(z)$; $c(z) \approx 20.067 \sqrt{T(z)}$; T is the absolute temperature of air, in K, $|\mathbf{a}| = k_0 \cos\alpha / \{1 + v_0/c_0 \cos\alpha \cos(\varphi_V - \varphi)\}$, $k_0 = \omega/c_0$, and $\omega = 2\pi f$. Here, the subscript 0 denotes the values of the parameters at the emission point of ray trajectory $\mathbf{R}_0(x_0, y_0, z_0)$. The angle of ray departure α is specified in the vertical plane as the angle between the normal to the wavefront phase at the point $\mathbf{R}_0$ and the horizon. The angles φ and φ_V specify the azimuthal directions of the given normal and the wind velocity $\mathbf{v}_0$, respectively. The vector $\mathbf{a}$ lies in the horizontal plane and is directed at

the angle φ. At each point of the ray this vector remains constant and is the horizontal component of the wave vector **K**(z).

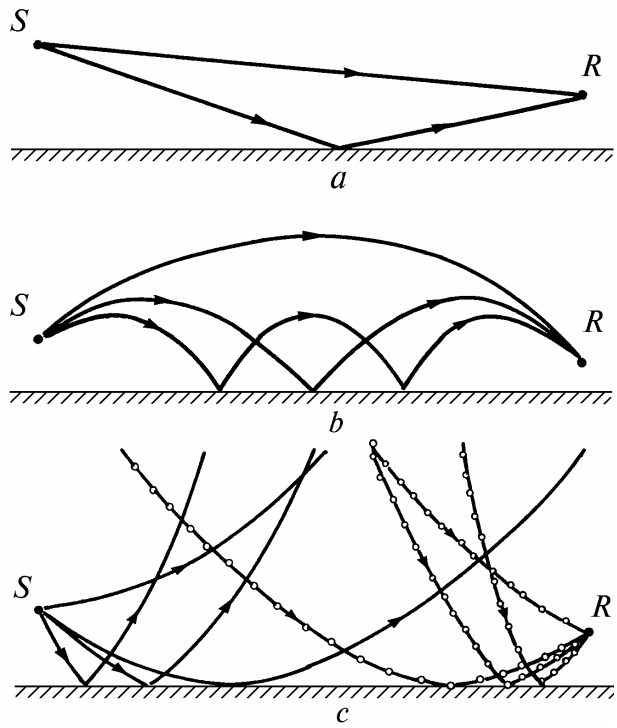

Figure 1: Ray patterns for sound propagation in the atmosphere under various meteorological conditions: a) neutral regime; b) waveguide regime (only the top–bottom rays are shown); and, c) nonwaveguide regime. Here *S* is the sound source, *R* is the receiver (observation point), ———, direct rays, °–°–°–, the scattered rays.

The ray path equation is correct in this form only for the portion of the ray path before the point of its bending. This equation is easy generalized to the case of ray bending at the point located at the altitude z_b by way of substitution

$$\int_{Z_0}^{Z'} \mathrm{d}\,z \to \left(\int_{Z_0}^{Z_b} + \int_{Z'}^{Z_b} \right) \mathrm{d}\,z\,,$$

where z' is the altitude of the end point of the ray path. Analogously, Eq. (2) is generalized to the case of several bending points when the ray undergoes multiple reflection from the earth surface.

In accordance with the ray classification given in (Brekhovskikh, 1973), for the case of waveguide propagation there are four types of rays depending on the portion of the ray trajectory (descending or ascending) at which a source and a receiver are located. In our software package the rays of the type top–bottom (see Figure 1*b*) provide the basis for calculation of sound pressure level. The characteristics of these rays are calculated by a direct solution of the exact ray path equation with the known number of bending points, while the characteristics of the other rays are calculated from the approximate relations using the results of the base ray calculations. In calculations of the energetic parameters, the other rays with the same number i, which cannot be classified as top–bottom, are taken into account as the correction

for interference $L_{e\,i}$ to the sound pressure level L_i produced only by the base ray having number i. For this purpose, the following relation (Abramov, 1988) is used:

$$L_e = -10 \cdot \log\left\{ e^{-2\sigma_\chi^2} \left[1 + Q^2 \cdot (s/s_0)^2\right] + 2Q(s/s_0) \cdot e^{2\sigma_\chi^2 - D_S(\Delta\rho)} \cos\left[k_0(s - s_0) + \theta\right]\right\},$$

where Q is the modulus of the amplitude coefficient of sound reflection from the underlying surface; θ is the phase of this coefficient; σ_χ^2 is the relative variance of log–amplitude fluctuations of acoustic signal in the atmosphere; D_s is the structure function for fluctuations of phase difference between the direct and reflected waves; s and s_0 are the propagation path lengths from the source to the receiver ($|s - s_0| < s, s_0$); $\Delta\rho$ is the effective transverse separation of these paths. The values σ_χ^2 and D_s are calculated here by the formulas from (Tatarskii, 1967), while Q and θ are calculated on the basis of the known Delany–Bazley model for the complex acoustic impedance of the underlying surface.

When calculating the base ray number i, the known quantities are the coordinates x' and y' of its end point and the number of bending points. Using these data, it is necessary to find the angles of departure α_i and φ_i of the ith ray, i.e. to aim this ray at the given point. Analytical solution of this problem cannot be derived from Eq. (2) for arbitrary profiles $c(z)$ and $\mathbf{v}(z)$. Therefore, to solve this problem, the dichotomy technique (Kalitkin, 1978) was used. By this algorithm, integral (2) is calculated repeatedly, thereby substantially increasing the execution time. The altitude of a bending point z_{bi} of the ith ray is calculated at each iteration from the equation $q(\alpha_i, \varphi_i, z_{bi}) = 0$ for the running angles of departure α_i and φ_i at the given iteration. In the solution of the problem of ray aiming we assume that $\varphi_i = \arctan(\bar{v}_\perp/c)$, where $\bar{v}_\perp$ is the mean transverse wind velocity along the ray path, and the iterative search is conducted only for the angle α_i. Numerical comparison with the exact ray trajectory shows that the errors of calculations of α_i and φ_i are much smaller than the angular width of the directional pattern of a real sound source, and hence have insignificant effect on the results of calculations of sound pressure levels. For example, for $d = 5$ km, $v = 12$ m/s, and an angle of 45° between the wind and ray path directions, the errors in estimating α_i and φ_i in this approximation take the values 0.6° and 0.5°, respectively.

After the determination of α_i and φ_i for all rays whose number $N_{\min} < i < N_{\max}$ ($N_{\min} \geq 1$, $N_{\max} \geq N_{\min}$), it becomes possible to calculate $L_{abs\,i}$, $L_{t\,i}$, $L_{e\,i}$, $L_{pat\,i}$, and $L_{div\,i}$, as well as Q_i. The quantity $L_{div\,i}$ is determined by calculation of the wave focusing factor for each ray at its end point (Brekhovskikh and Lysanov, 1982). Due to multipath sound propagation in the given regime, the equation of energy balance is complicated and has the form

$$L_r(f) = L_s(f) + 10 \log\left[\sum_{i=N_{\min}}^{N_{\max}} \left(Q^{2(i-1)} \cdot 10^{L_{\Sigma i}(f)/10}\right)\right], \text{ dB} \qquad (3)$$

where, in analogy with Eq. (1), $L_{\Sigma\,i} = L_{abs\,i} + L_{t\,i} + L_{e\,i} + L_{pat\,i} + L_{div\,i}$. Because $Q_i < 1$, it is sufficient to take into account only three or four first terms in Eq. (3) in approximate calculations. The error in estimating L_r in this case is no more than 0.1 dB.

3 ALGORITHM FOR CALCULATING THE SOUND PRESSURE LEVEL IN A SHADOW ZONE

The algorithm is based on the theory of single scattering of sound in the atmosphere (Ostashev, 1992; Tatarskii, 1967; Rytov et al., 1978) and geometric acoustics equations for moving media (Ostashev, 1992; Blokhintzev, 1981).

It is well known (Rytov et al., 1978) that the average intensity of a scattered field produced in the medium by the sound pulse described by the function of time $M(t)$ can be estimated in the Born approximation as

$$I_r(t) = I_0 \cdot \int_V \Pi(\mathbf{R}) \cdot M[t - \tau(\mathbf{R})]\sigma(\theta, \mathbf{R})\mathrm{d}\, z\,, \tag{4}$$

where the integral is taken over the points **R** of the scattering volume V. Here, I_0 is the amplitude factor independent of t and **R**, $\tau(\mathbf{R})$ is the time of sound ray propagation along the path of length $s(\mathbf{R})$ from the source to the receiver with scattering at the point **R**, and $\Pi(\mathbf{R})$ is the weighting function of the scattering volume allowing for total energetic sound losses. In the examined case, this function can be represented in the form

$$\Pi(\mathbf{R}) = F[\alpha_1(\mathbf{R}) - \alpha_0, \varphi_1(\mathbf{R}) - \varphi_0]\, F_f(\mathbf{R})\, F_e(\mathbf{R}) \exp[-\alpha_\Sigma\, s(\mathbf{R})], \tag{5}$$

where F describes the source directional pattern that depends on the difference between the angles of departure of the direct ray α_1 and φ_1 aimed at point **R** and the angles α_0 and φ_0 at which the source directional pattern reaches its maximum, F_f is the factor that considers refractive losses and losses caused by spherical divergence, F_e is the factor that considers sound attenuation by the ground due to interference between the directly transmitted ray and the ray reflected from the ground (Abramov, 1988), and α_Σ is the total attenuation coefficient caused by classical and molecular absorption and turbulent attenuation of sound (Krasnenko, 1986).

One or more pair of direct rays 1 and scattered rays 2 correspond to each jth scattering point $\mathbf{R}_j$ being the nodal point in numerical integration of Eq. (4) (see Figure 1*c*). Therefore, in our calculations the zenith (α_1) and azimuth (φ_1) angles of departure of the direct ray together with the zenith angle of arrival of the scattered ray (α_2) were chosen as variables of integration in Eq. (4). In this case, the problem of sound refraction reduces to the calculation of the azimuth angle φ_2 and the vertical coordinate z_j of the point $\mathbf{R}_j$ for the given parameters α_1, φ_1, and α_2 from the system of equations

$$x_{1j} + x_{2j} = d, \quad y_{1j} + y_{2j} = 0, \tag{6}$$

where x_{1j} and y_{1j} are the projections of the direct ray propagating from the source to the point $\mathbf{R}_j$ onto the axes **X** and **Y**, respectively; x_{2j} and y_{2j} are analogous projections for the scattered ray propagating from point $\mathbf{R}_j$ to the observation point spaced at the distance d from the source along the axis **X**. These projections can be both positive and negative as functions of the position of the point $\mathbf{R}_j$. They were calculated with the use of Eq. (2) for a sound ray in a stratified moving medium. We failed to derive the analytic solution to Eq. (2) for arbitrary profiles $T(z)$ and $\mathbf{v}(z)$ and solved the problem numerically by the method of dichotomy (Kalitkin, 1978). The other coordinates of the point $\mathbf{R}_j$ can be easily found for the known value of z_j using Eq. (2).

In the geometric acoustics approximation, the sound energy conservation law leads to the expression (Ostashev, 1992)

$$I\,\mathrm{d}S = \text{const}, \tag{7}$$

where $\mathrm{d}S$ is the cross section area of an infinitely narrow ray tube. We now demonstrate how to calculate the focusing factor $F_F(\mathbf{R}_j)$ in Eq. (4). Let us look at Figure 2 that shows schematically in the vertical plane the volume scattering element dV formed by intersection of two infinitely narrow ray tubes, with the first ray being the direct ray and the second ray being the scattered ray. At small distance from the source R_0,

when the refraction can be neglected, the cross section area of the first tube is $dS_1(\mathbf{R}_0)=R_0^2 \cdot d\alpha_1 \cdot d\varphi_1$. If we introduce the sound intensity I_0 recorded at the distance $R_0 = 1$ m from the antenna aperture as a standard characteristic, we will derive from Eq. (7)

$$I(\mathbf{R}_j) = I_0 \, d\alpha_1 \, d\varphi_1 / dS_1(\mathbf{R}_j). \tag{8}$$

Because from Figure 2 it follows that $dS_1(\mathbf{R}_j) \approx l_1 \cdot \sin\xi_j \cdot s_{1j} \cdot d\varphi_1$, where s_{1j} is the length of the tube from the source to the point $\mathbf{R}_j$, ξ_j is the angle between the direct and scattered rays at the point $\mathbf{R}_j$, Eq. (8) can be written as follows:

$$I(\mathbf{R}_j) \approx I_0 \, d\alpha_1 / (l_1 \, s_{1j} \sin\xi_j). \tag{9}$$

Analogous equation also can be obtained for the second ray tube:

$$dI_r \approx I'(\mathbf{R}_j) \, d\alpha_2 / (l_2 \, s_{2j} \sin\xi_j), \tag{10}$$

where $I'(\mathbf{R}_j) = I(\mathbf{R}_j) \cdot \sigma(\theta_j, \mathbf{R}_j) \cdot dV$ is the intensity of sound scattered by the volume element dV at the angle θ_j. Substituting Eq. (9) into Eq. (10) on account of Eqs. (4) and (5), we derive

$$F_{fj} \approx d\alpha_1 \, d\alpha_2 / (s_{1j} \, s_{2j} \, l_1 \, l_2 \sin^2\xi_j). \tag{11}$$

The main difficulties arise in calculations of l_1 and l_2 that specify refraction focusing of the ray tubes in Eq. (11). However, it can be seen from Fig. 2 that $dV \approx l_1 \cdot l_2 \cdot s_{1j} \cdot d\varphi_1 \cdot \sin\xi_j$. In so doing, it turns out that the product

$$F_{fj} \, dV \approx d\alpha_1 \, d\varphi_1 d\alpha_2 / (s_{2j} \sin\xi_j) \tag{12}$$

is independent of l_1 and l_2.

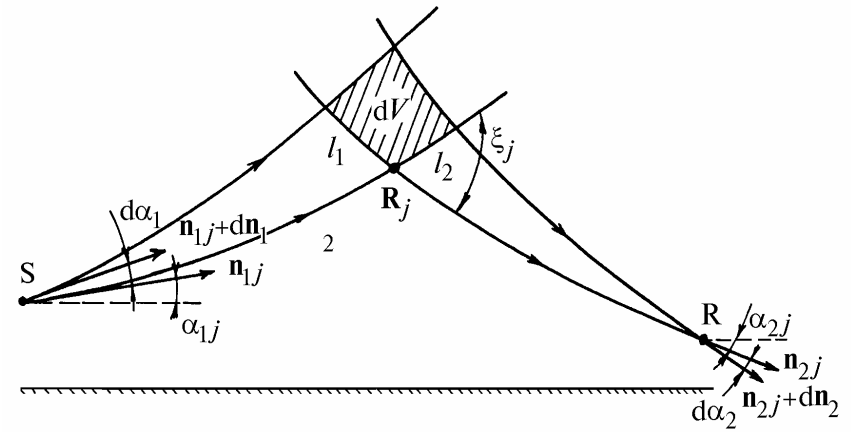

Figure 2: To the calculation of the focusing factor and the scattering volume element.

Thus, in Eq. (4) the choice of the parameters α_1, φ_1, and α_2 as integration variables results in the nonuniform distribution of nodal points of integration $\mathbf{R}_j$, for which the volume scattering element is nearly inversely proportional to the focusing factor. This remarkable fact decreases significantly (several times) the time of computation of this integral. It should be noted that Eq. (12) does not take into account the sound ray curvature in the azimuth plane. However, in a stratified medium for small α_1 and α_2 it is much less important than the ray curvature in the vertical plane. Therefore, the error in calculating the sound pressure level by Eq. (12) is small.

In our experiment we measured the sound pressure level. For this reason, we should eliminate the sound intensity I from Eq. (12) using the formula (Ostashev, 1992)

$$I = p^2 (1 + \mathbf{n}\,\mathbf{v}/c)\, U(2\rho c), \tag{13}$$

where p is the sound pressure level, in Pa, $U = |c\mathbf{n} + \mathbf{v}|$ is the group velocity of sound, and ρ is the air density.

Let the sound pressure level at a distance of 1 m from the source aperture be p_0. Then by virtue of Eq. (13) we obtain

$$I_0 = p_0^2 g_1/(2\rho_1 c_1),$$

where

$$g_1 = [1 + v_1/c_1 \cos\alpha_1 \cos(\varphi_V - \varphi_1)]\,[c_1^2 + 2\, v_1/c_1 \cos\alpha_1 \cos((\varphi_V - \varphi_1) + v_1^2]^{1/2}.$$

Analogously, for the intensity of sound scattered by the volume element dV we have

$$\mathrm{d}I_r = \mathrm{d}\, p_r^2 g_2/(2\rho_2 c_2),$$

where the formula for g_2 is written analogously to that for g_1. In the first case, we substitute the parameters of the medium c, $\mathbf{v}$, and ρ for the point of the direct ray emission, whereas in the second case ~ for the end point of the scattered ray. On account of the two last formulas and Eqs. (5) and (12), the computational formula

$$L_r = L_0 + 10 \cdot \lg\left\{ \frac{\rho_2 \cdot c_2}{\rho_1 \cdot c_1} \int_{\alpha_{1\min}}^{\alpha_{1\max}} \int_{\varphi_{1\min}}^{\varphi_{1\max}} \int_{\alpha_{2\min}}^{\alpha_{2\max}} \hat{F}(R_j)\, \mathrm{d}\alpha_1 \mathrm{d}\varphi_1 \mathrm{d}\alpha_2 \right\}, \tag{14}$$

where

$$\hat{F}(\mathbf{R}_j) \approx g_1(\alpha_1, \varphi_1)/[g_2(\alpha_2, \varphi_2)\, s_2(\mathbf{R}_j) \sin\xi_j]\, F(\alpha_1 - \alpha_0, \varphi_1 - \varphi_0) \times$$

$$\times M[\tau_i/2 + \tau_{\min} - \tau(\mathbf{R}_j)]\, F_e(\mathbf{R}_j) \exp[-\alpha_\Sigma s(\mathbf{R}_j)]$$

was derived from Eq. (4).

This formula can be used to estimate numerically the peak sound pressure level. To this end, the time of sound propagation $\tau_{\min}$ along the rays with zenith angles of departure ($\alpha_{1\min}$ and ($\alpha_{2\min}$ and $\varphi_1 = 0$ is additionally calculated that enters the function $M(\cdot)$. The energetic losses are minimum for these rays. Here, time $t = \tau_i/2 + \tau_{\min}$ from the instant of transmission of pulse with duration τ_i corresponds to the instant of recording the maximum scattered signal amplitude. The above equation (14) is solved for φ_2 and coordinates $\mathbf{R}_j$ with each combination of the parameters α_1, φ_1, and α_2 used in numerical integration. A separate problem that is not considered in the present paper is the computation of the angles ξ and θ in the point $\mathbf{R}_j$ for the given α_1, φ_1, and α_2 and profiles $T(z)$ and $\mathbf{v}(z)$. The procedure for its numerical solution

based on the exact equations of geometric acoustics was described by us in (Bogushevich and Krasnenko, 1994). The angles α_{1min} and α_{2min} were specified in Eq. (14) for the direct and scattered rays tangent to the Earth's surface for $\varphi_1 = 0$ (see Figure 1c); the angles α_{1max}, φ_{1min}, and φ_{1max} were determined from the source directional pattern F at a level of 0.1 from its maximum; the angle α_{2min} was determined from the condition $\theta < 90°$ (in the atmosphere, the intensity of sound scattered at angles $90 \le \theta \le 180°$ is much less than that scattered in the forward hemisphere). The rays with angles of departure $\alpha_1 < \alpha_{1min}$ and $\alpha_2 < \alpha_{2min}$ were considered in Eq. (14) in the process of calculations of the factor of attenuation by the ground $F_e(\mathbf{R}_j)$.

4 SOFTWARE PACKAGE OUTDOOR ACOUSTICS

The above algorithms were used to develop the software package Outdoor Acoustics (OA) intended for real-time estimation of the sound pressure level in the range of audible frequencies for observation points located at distances up to 10 km from the source. The flowchart of this software package is shown in Figure 3.

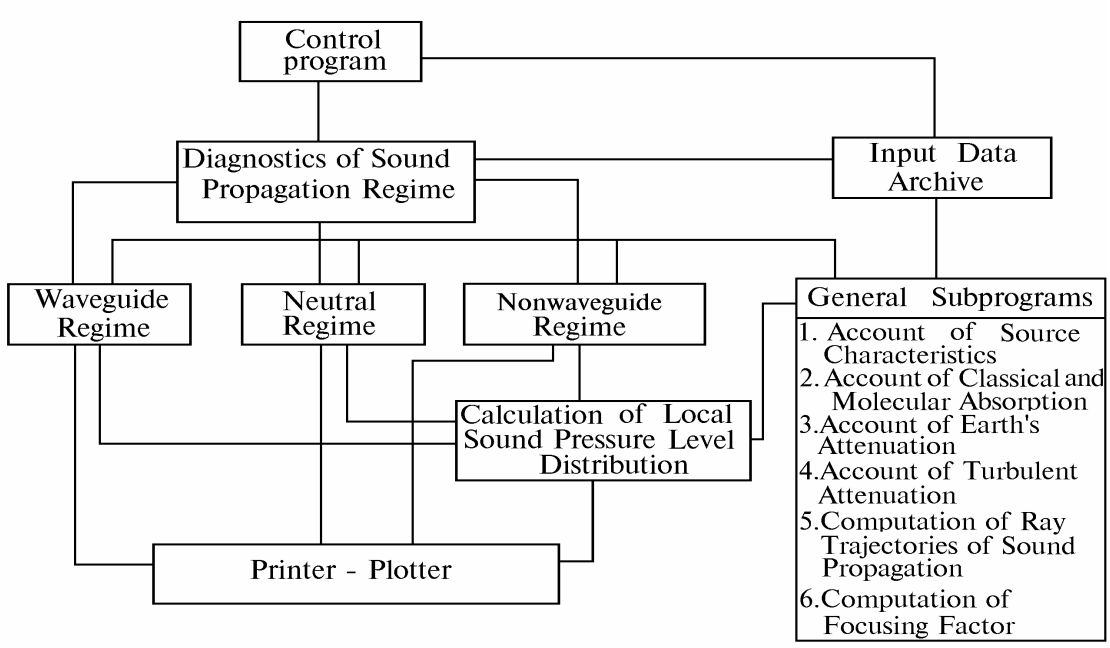

Figure 3: Flowchart of the software package OA (Outdoor Acoustics).

In the forecast problems, the initial data are the four groups of input parameters: meteorological, underlying surface, source, and propagation path. Among the meteorological parameters, the velocity v and direction φ_v of horizontal wind component, the temperature T and the relative air humidity u, the atmospheric pressure p_a, the structure constants for turbulent fluctuations of temperature C_T^2 and wind velocity C_V^2 are considered in this package. Diagnostics of sound propagation regime is based here on an analysis of the altitude distribution of the sign of the phase velocity gradient of sound wave.

When calculating the above–considered regimes of sound propagation, the ray patterns are displayed and the amplitude–frequency characteristic of sound at the given point is tabulated for one–third octave intervals on the screen of a monitor. Some parameters characterizing the given regime are also displayed. Moreover, the software package comprises an additional program for calculation and graphics of diagrams of distribution of the sound pressure levels in the neighborhood of the source.

The efficiency of this package was tested for distances d varying from 100 m to 10 km for various wind velocities up to 25 m/s and temperature gradients varying from -40 deg/km to $+40$ deg/km. The computational error in estimating the sound pressure level for waveguide regime was 0.1 dB. It was 0.5 dB for nonwaveguide regime. The greater error in the last case was due to the increased volume of computations and was a reasonable compromise between the accuracy and the execution time. The package includes original algorithms substantially decreasing the execution time.

The sensitivity of the accuracy of the forecast to the errors in assignment of meteorological information was also considered. It turns out that the error in the predicted sound pressure level is no more than 1 dB if p_a is assigned with the error no more than 100 mm Hg; v and φ_v are assigned with the errors no more than 0.5 m/s and 10°, respectively; T is assigned with the error no more than 1°; and, u is assigned with the error no more than 10% in calculation at the frequencies below 2 kHz and no more than 3% in calculation in the frequency range 2–4 kHz. The relative errors of assignment of C_T^2 and C_V^2 did not exceed 300% in calculation of the neutral and waveguide regimes and 100% of the nonwaveguide regime. It has been found that changes in p_a and u with altitude may be neglected. This is justified for C_T^2 and C_V^2 in the calculation of the neutral and waveguide regimes only. The vertical profiles of v, φ_V, T, and C_T^2 and C_V^2 must be assigned in calculation of the waveguide regime. In this case, the high sensitivity is observed to the accuracy of assignment of their gradients. For example, the temperature gradient must be assigned with the accuracy no less than 10^{-3} deg/m.

5 EXPERIMENTAL DATA

The software package has passed the field tests. In the experiments the acoustic system radiating a power of 1.8 kW and including the array of $6\times4 = 24$ horn loudspeakers and 6 power amplifiers with a standard mixer panel was used. The mean sound pressure level recorded at a distance of 1 m from the source was about 138–147 dB in the frequency range from 315 Hz to 4 kHz. Three stations of acquisition of the data on the sound pressure level measured by operators with the use of a sound level meter and octave filters were organized along the two near–ground paths of sound propagation of length up to 6 km. To monitor the atmospheric state a two–level device for measuring the meteorological parameters (DMP) and the Mars radar station were used. The station gave the values of the meteorological parameters at altitudes of 0, 200, 400, 800, and 1200 m.

An acoustic signal was radiated as a train of 20 pulses whose duration was about 0.5 s and the time intervals between pulse trains were 2 s. This pulse train was repeatedly radiated with one–third octave intervals from 315 Hz up to 4 kHz. Then the first cycle of measurements whose duration was about 25 minutes terminated. In all, 33 cycles of measurements corresponding to the case of waveguide sound propagation and 19 cycles of measurements, when operators were within the acoustic shadow zone, were carried out. In every cycle the values of sound pressure level $L_r(f)$ averaged over 20 measurements were obtained at all frequencies f and various distances d to the point of measurement. The variances and confidence intervals of these values (with a confidence level of 0.95) were also obtained. The error in forecasting $S(f)$ at the frequency f was estimated as the difference between the calculated values of $L_r(f)$ and the measured ones.

The examples of comparison of the calculated values of sound pressure level and experimental ones for one measurement cycle in the case of waveguide and nonwaveguide regimes, respectively, are shown in Figures 4 and 5. Due to strong sound attenuation at frequencies above 2 kHz, the signal at these frequencies was typically lower than the level of the ambient noise. Therefore, the experimental data for the given path lengths d were largely obtained only for the frequency range 315–2000 Hz.

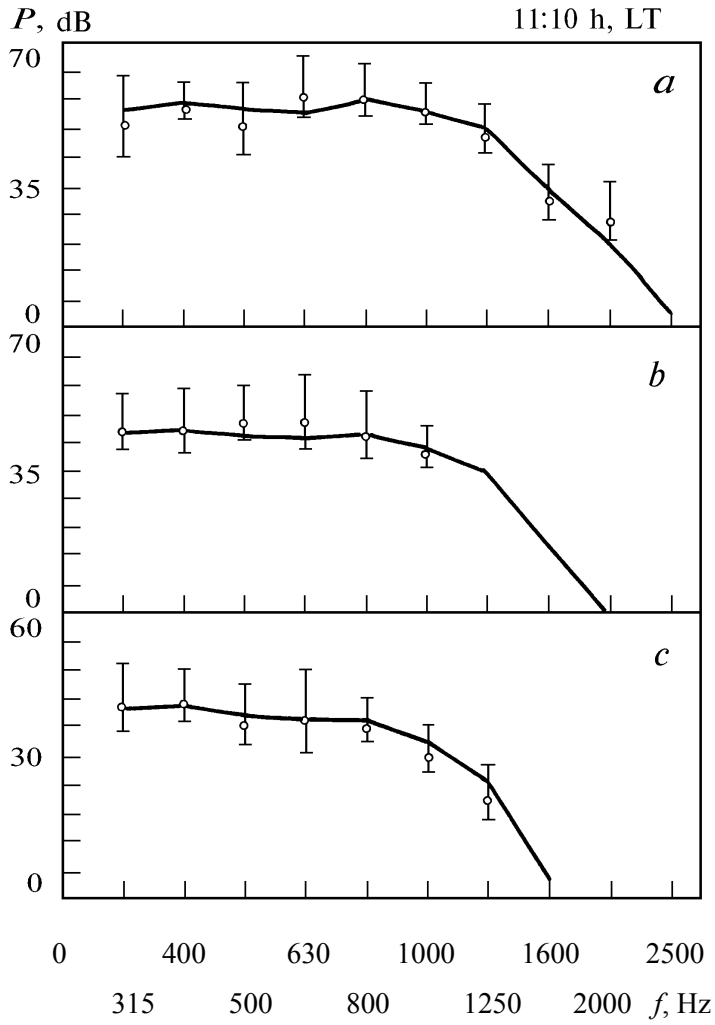

Figure 4: Sound pressure level, in dB, in the case of waveguide regime for different path lengths as a function of the frequency *f* of radiated signal for *d* = 3000 (a), 4500 (b), and 6000 m (c). Solid curves are for the calculated results; circles are for the measured values. Vertical bars denote a 95% confidence intervals.

On the whole, the frequency dependences of the calculated and measured values of sound pressure level in this frequency range agree fairly well.

It was found in the experiments that the main source of errors is the inaccuracy in assignment of meteorological information. The revealed errors of assignment of this information can be divided into three groups. First, the meteorological data came from the radar station at relatively large nearly two–hour intervals. The time of acquiring the information about the sound pressure level in one measurement cycle indicated above was larger than the interval usually considered as the period of meteorological field stationarity. Therefore, under unstable meteorological conditions when the mean profiles of the meteorological parameters undergo large and relatively fast variations, the quality of the forecast in our experiments must decrease.

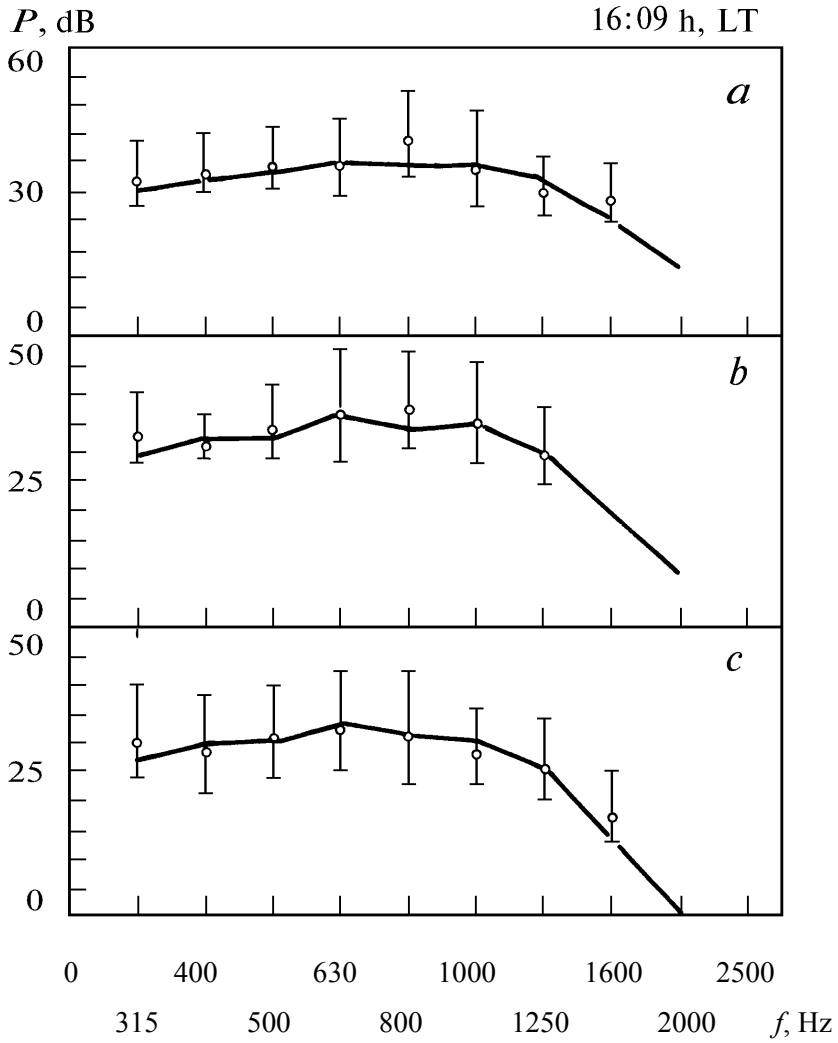

Figure 5: Sound pressure level, in dB, in the case of nonwaveguide regime for various path lengths as a function of the frequency f of radiated signal for $d = 3575$ (a), 4135 (b), and 4800 m (c). Solid lines are for the results of calculation, and circles are for the measured values. Vertical bars denote a 95% confidence intervals.

Second, there is a systematic error associated with the assumption of horizontal homogeneity of meteorological fields in the atmosphere. At last, instrumental errors are always present.

In the experiments the stable meteorological conditions predominated. Usually the wind was about 5–7 m/s at an altitude of 2 m. The variance of the wind direction was small. The negative temperature gradient of the order of 8–10 deg/km was typically observed.

The results of experimental estimation of the efficiency of forecast of the sound pressure level in the frequency range 315–2000 Hz for different distances and propagation regimes are summarized in Table I. Here, $\bar{S}$ is the error in forecast averaged over all cycles; P_i is the probability that the predicted pressure level is in the confidence interval; P_6 is the probability that the error in forecasting is no more than 6 dB. On account of the difficulties of monitoring of meteorological conditions and their variability, the obtained 2–3 dB mean errors of forecast are sufficiently good results.

Table I: Experimental results.

Waveguide regime, 33 cycles × 20 pulse trains				Nonwaveguide regime, 19 cycles × 20 pulse trains			
d, m	$\overline{S}$, , dB	P_6	P_i	d, m	$\overline{S}$, , dB	P_6	P_i
3000	+3.2	0.67	0.67	3575	–2.3	0.83	0.78
4500	+2.3	0.67	0.68	4135	–2.3	0.82	0.75
6000	+1.5	0.80	0.74	4800	–1.5	0.82	0.82

6 NUMERICAL ESTIMATION OF THE INFLUENCE OF METEOROLOGICAL CONDITIONS ON SOUND ATTENUATION

An attempt was made to analyze numerically, with the use of this software package, the effect of the meteorological parameters on audibility of sound in the atmosphere. The most interesting results of calculations are shown in Figs. 6–9. The values of the main atmospheric parameters at a height of 2 m above the ground are indicated in figure captions. The vertical wind velocity profile was assumed to be logarithmic in character, the air humidity and pressure were constant, the vertical profile of C_n^2 was determined by the corresponding profiles of C_T^2 and C_V^2, and the underlying surface was covered with grass.

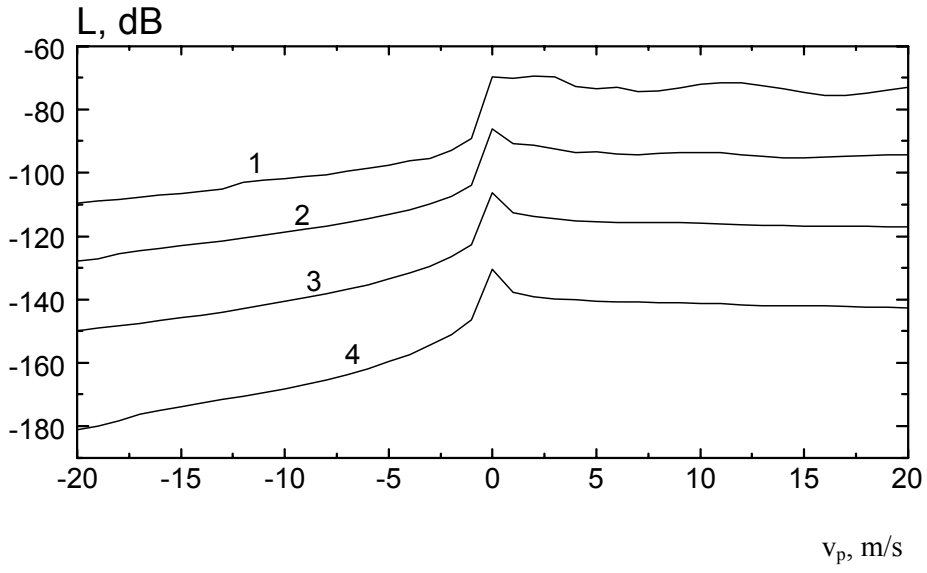

Figure 6: Dependence of sound attenuation in the atmosphere, in dB, on the wind component v_p parallel to the direction of sound propagation for P_a = 750 mm Hg, u = 75%, T = 20°C, γ = 0°/km, $C_n^2 = 10^{-6}$ m$^{-2/3}$, f = 1000 Hz, and distances to the source d = 1 (1), 3 (2), 6 (3), and 10 km (4).

The dependence of the total attenuation L on the wind component parallel to the direction of sound propagation v_p is shown in Fig. 6. Here, the waveguide regime of propagation is realized for $v_p > 0$ and the nonwaveguide regime – for $v_p < 0$. Refraction by wind velocity gradients always results in the increase of sound attenuation. In the waveguide regime of propagation, the increase of v_p is accompanied by a relatively small increase in $|L|$, as a rule, by no more than 6–10 dB, connected with the change of the beam focusing pattern compared with the conventional spherical beam divergence. At the same time, in the nonwaveguide regime of propagation, the excess noise attenuation due to wind is much greater and may even exceed 100 dB. In this case, the sharp increase of $|L|$ by 15–20 dB is first observed as $|v_p|$ increases and the observation point enters the acoustic shadow zone. With the further increase of $|v_p|$, the sound attenuation continues to increase noticeably, because the atmospheric layer, from which a scattered signal comes to the observation point, is displaced upward. The change of the distance from the source d affects insignificantly the form of the dependence $L(v_p)$, but shifts noticeably the absolute values of L.

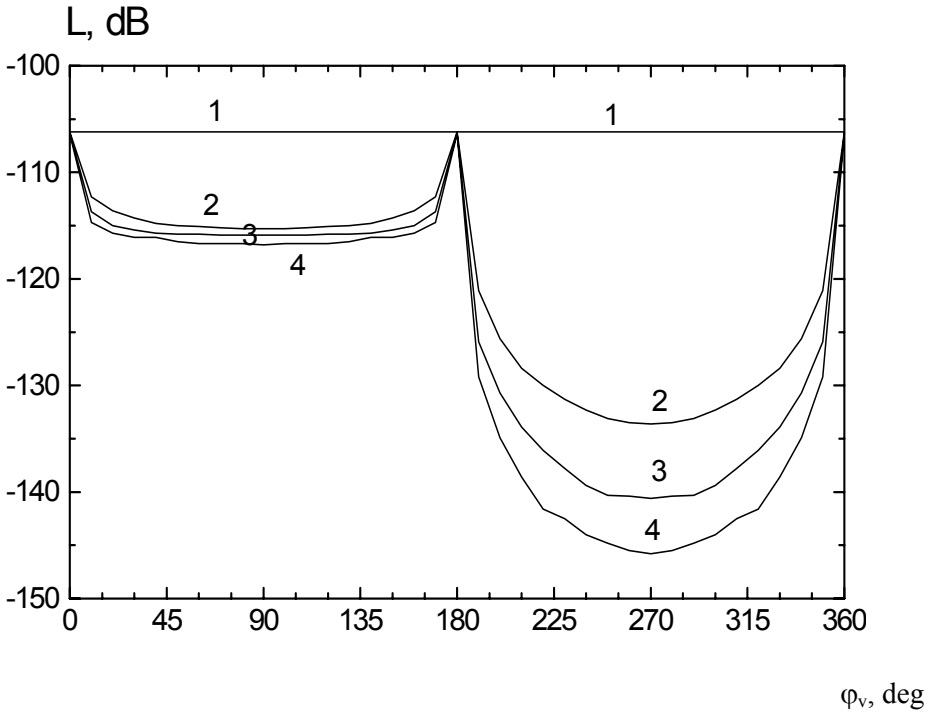

Figure 7: Sound attenuation in the atmosphere, in dB, as a function of the wind direction φ_v for $u = 75\%$, $T = 20°C$, $\gamma = 0°/km$, $C_n^2 = 10^{-6}$ m$^{-2/3}$, $f = 1000$ Hz, and $\mathbf{v} = |\mathbf{v}| = 0$ (1), 5 (2), 10 (3), and 15 m/s (4).

Figure 7 shows sound audibility as a function of the wind direction φ_v counted off from the source-observer direction. Curve *1* was calculated without refraction ($v = 0$). It can be easily seen that at $\mathbf{v} = const$ the change of φ_v is equivalent to the change of the wind component v_p parallel to the direction of sound propagation. Therefore, curves *2*, *3*, and *4* exhibit practically the same behavior as in Fig. 6. From Fig. 7 it follows that the wind component perpendicular to the direction of sound propagation affects insignificantly its audibility.

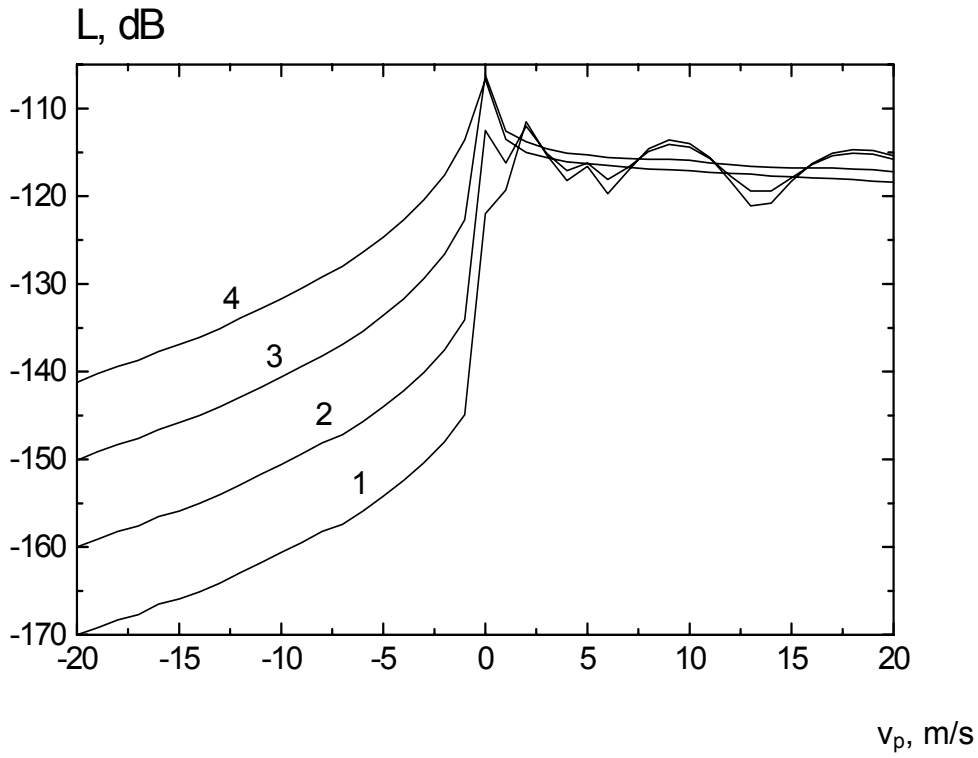

Figure 8: Sound attenuation in the atmosphere, in dB, as a function of the wind component v_p parallel to the direction of sound propagation for $u = 75\%$, $T = 20°C$, $\gamma = 0°/km$, $f = 1000$ Hz, $d = 6$ km, and $C_n^2 = 10^{-8}$ (1), 10^{-7} (2), 10^{-6} (3), and 10^{-5} $m^{-2/3}$ (4).

Figure 8 shows the dependence of L on v_p for indicated values of the structure parameter of refractive index fluctuations C_n^2 that characterize the intensity of the atmospheric turbulence. As expected, C_n^2 affects most strongly the sound pressure level in the nonwaveguide regime of propagation. In this case, the recorded pressure level is almost proportional to C_n^2. Because C_n^2 varies over a wide range, sound audibility also undergoes large variations. In our case experimental values changed from 2 to 5 km.

In the waveguide regime of propagation, the observed sound pressure level is a sum of pressure levels of individual rays propagating along paths of different lengths. The total pressure level differs qualitatively as a function of amplitude and phase fluctuations of rays. For small values of C_n^2, the amplitude and phase fluctuations of rays are also small and hence can be partly coherent. In this case, because the ray path lengths depend on the **v** profile, the linear increase of v_p results in the interference sound pressure pattern vividly seen in Figure 8 for curves *1* and *2*. For large values of C_n^2, the rays are incoherent and interference is not observed. Coherence starts to break at smaller values of C_n^2 as the distance between the source and the receiver increases.

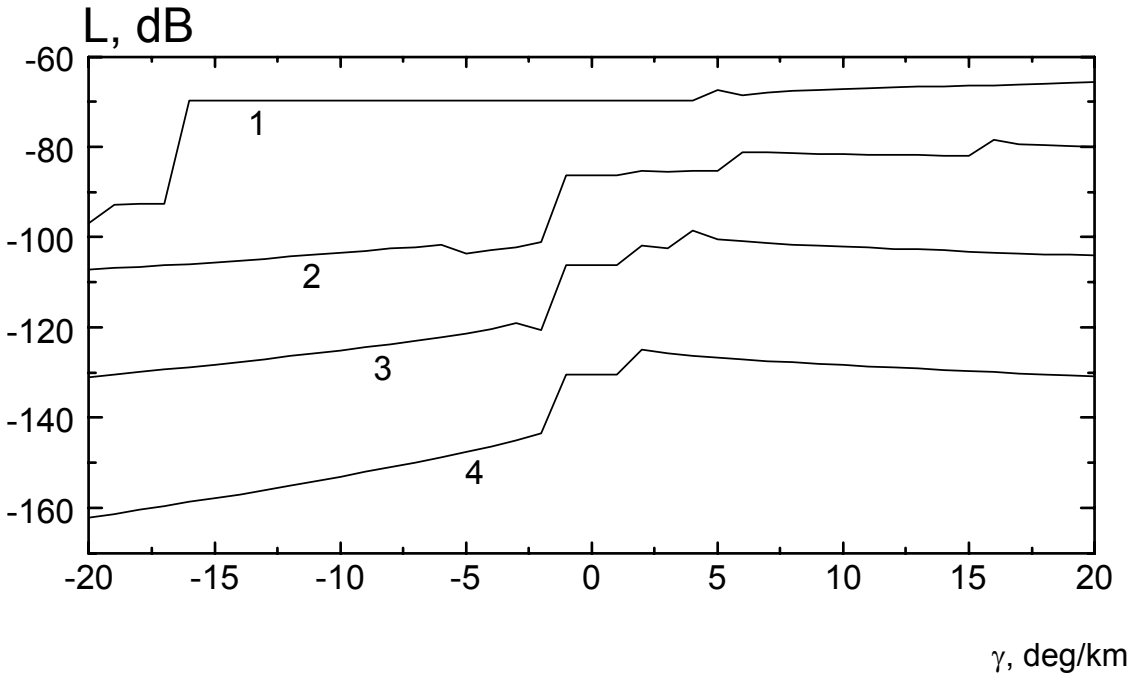

Figure 9: Sound attenuation in the atmosphere, in dB, as a function of the temperature gradient γ for u = 75%, T = 20°C, $C_n^2 = 10^{-6}$ m$^{-2/3}$, f = 1000 Hz, and d = 1 (1), 3 (2), 6 (3), and 10 km (4).

The effect of temperature gradient on sound attenuation in the atmosphere is illustrated by Figure 9. For $\gamma > 0$, the waveguide regime of sound propagation is realized, as in the case of wind refraction for $v_p > 0$, but in contrast to it, additional beam focusing takes place resulting in sound amplification. Therefore, the presence of temperature inversion in the atmosphere increases the sound level. In calculations, the sound source was at $r_1 = 5$ m above the ground and the observation point was at $r_2 = 1.5$ m. In the nonwaveguide regime of sound propagation, the zone of line-of-sight propagation always exists in the vicinity of the source followed by the acoustic shadow zone. For high source and receive the distance to this shadow zone is determined by the curvature radii of ray paths, which are noticeably smaller in case of refraction by temperature gradients than in case of refraction by wind gradients. Therefore, when $\gamma < 0$ and the observation point is in the shadow zone, the sharp increase of sound attenuation takes place for large absolute values of γ. The further increase of the sound attenuation in the shadow zone as $|\gamma|$ increases is caused by the upward displacement of the lower boundary of the region of sound scattering, as in the case of wind refraction.

8 CONCLUSION AND RECOMMENDATION

The sound pressure level from a remote source has been estimated. Significance of the influence of different atmospheric parameters also has been demonstrated. Good accuracy of sound pressure level prediction has been obtained in the field test. A wide application area of the above-described algorithms and software package Outdoor Acoustics for routine prediction of the sound pressure level should be emphasized. This software package can be used successively for routine evalution of the sound pressure level at the observation point, study of the noise background in the atmosphere produced by newly developed devices, calculation of the extension of sanitary zones of industrial objects against the criterion of the noise pressure level produced in the atmosphere, mapping of noise intensity distribution in populated areas, estimation of audibility of sound sources, etc.

9 REFERENCES

Abramov, N.G., 1988: Intensity fluctuations of a sound wave that propagates near the ground. *Propagation of Sound and Optical Waves through the Atmosphere.* Tomsk: IAO Publishing House, 97–100.

Abramov, N.G., Bogushevich, A.Ya., Karpov, V.I., Krasnenko, N. P., Fomichev, A.A., 1994: Feasibility of routine forecast of propagation of the acoustic noise in the ground atmospheric layer with allowance for meteorological conditions. *Atmos. Oceanic Optics*, **7**, 215–220.

Blokhintzev, D.I., 1981: *Acoustic of an Inhomogeneous Moving Medium.* Moscow: Nauka, 208 pp.

Bogushevich, A. Ya., Krasnenko, N. P., 1993: Operative forecast of acoustic noise propagation along ground surface through atmosphere taking into account meteorological condition. *Proc. INTER-NOISE' 93*, Leuven, Belgium, **3**, 1751–1754.

Bogushevich, A. Ya., Krasnenko, N. P., 1994: Influence of refraction on sodar-derived atmospheric parameters. *Atmos. Oceanic Optics,* **7**, 1258–1274.

Bogushevich, A. Ya., Krasnenko, N. P., 1996: Evaluation of the structural constant of the acoustic refractive index in the atmospheric boundary layer from the sound pressure measured in the shadow region. *Acoustical Physics*, **42**, 339–346.

Bogushevich, A. Ya., Krasnenko, N. P., 1997: The influence of atmospheric channel of the sound propagation on the noise control problems. Proc. *INTER–NOISE' 97*, Budapest, Hungary, **1**, 343–346.

Bogushevich, A., Krasnenko, N., 1998: Influence of the atmospheric channel on the sound propagation above the ground surface. *Proc. 9th Int. Symp. Acoust. Rem. Sens.*, Vienna, Austria, 19–22.

Brekhovskikh, L.M., 1973: *Waves in Stratified Media*. Moscow: Nauka, 342 pp.

Brekhovskikh, L.M., Lysanov, Ya.P., 1982: *Theoretical Principles of Acoustics of the Ocean.* Leningrad: Gidrometeoizdat, 264 pp.

Brown, E.H., and Hall, F.F., 1978: Advances in atmospheric acoustics. *Rev.Geophys. and Space Phys*., **16**, 47–110.

Harris, C.M., 1966: Absorption of sound in air versus humidity and temperature. *J. Acoust. Soc. Am.*, 40, 148–159.

Ingard, U., 1953: A review of the influence of meteorological conditions on sound propagation. *J. Acoust. Soc. Am.*, **25**, 405–411.

Kalitkin, N.N., 1978: *Numerical Techniques.* Moskow: Nauka, 512 pp.

Krasnenko, N.P., 1986*: Acoustic Sensing of the Atmosphere*. Novosibirsk: Nauka, 167 pp.

Ostashev, V.E., 1989: Ray acoustics in moving media. *Atmos. Oceanic Physics. Izv. Acad. Sci., USSR*, **25**, 899–916.

Ostashev, V.E., 1992: *Propagation of Sound in Moving Media*. Moscow: Nauka, 206 pp.

Rytov, S. M., Kravtsov, Yu. A., Tatarskii, V. I., 1978: *Introduction into Statistical Radio Physics*. Moscow: Nauka, **2**, 469 pp.

Tatarskii, V.I., 1967: *Wave Propagation through the Turbulent Atmosphere*. Moscow: Nauka, 548 pp.